On Wind-Driven Mixed Layers with Strong Horizontal Gradients—A Theory with Application to Coastal Upwelling

R. A. DE SZOEKE AND J. G. RICHMAN

College of Oceanography, Oregon State University, Corvallis, OR 97331

(Manuscript received 1 August 1983, in final form 1 November 1983)

ABSTRACT

A theory of a two-dimensional wind-driven diabatic ocean mixed layer with strong horizontal gradients is formulated analytically. An equation that allows the relaxation of the strict Ekman balance—Coriolis force against wind stress—is derived from a careful consideration of the cross-gradient momentum balance. The relaxation scale depends implicitly on mixed-layer depth and density distributions, which themselves are determined by mixing, entrainment and diabatic processes, and in simple situations reduces to the familiar baroclinic Rossby radius of deformation. When mixed-layer depth or density contrast at the mixed-layer base becomes small, this relaxation scale becomes small and characterizes the width of high-gradient front-like features in the mixed layer.

The theory is applied to the situation of coastal upwelling. The reduced mixed-layer equations are solved numerically. Wind-driven motion divergence, initially on the scale of the Rossby radius, O(10 km), is induced by the presence of a coastline, and thins the mixed layer. Entrainment mixes lower layer water, virtually undiluted, into the surface water and drastically reduces the vertical density contrast. These twin effects reduce the width of the upwelling zone, consistent with scaling arguments. A front forms between dense upwelled water and light offshore water in the time that the vertical velocity associated with the coastal motion divergence takes to bring the pycnocline to the surface, roughly 20 h in typical situations. Then the front is advected offshore by typical mixed-layer velocities, of order 3 cm s^{-1}. Numerical solutions confirm the suggestion of scaling arguments that the horizontal width of the front is very narrow, though finite—of order of 100 m. There is a slight double-celled circulation associated with this front, with motion convergence in the mixed layer inshore of it and divergence on its offshore edge.

1. Introduction

In this paper we take up the problem of formulating a consistent analytical model of rapid horizontal variations in a surface mixed layer in the ocean. We shall see that the central difficulty concerns the sensitive balance of momentum across the direction of maximum horizontal gradient between inertial acceleration, Coriolis acceleration, and imposed wind stress. The momentum balance along the direction of the gradient is geostrophic. This is similar to the semigeostrophic dynamics that Hoskins and Bretherton (1972) and Hoskins (1975) developed for models of atmospheric fronts and that Pedlosky (1978) applied to an adiabatic model of the onset of coastal upwelling. The difference lies in the inclusion of wind-stress forcing, diabatic processes, and mixing processes in the dynamics of the surface boundary layer. Mixing processes are handled by generalizing the ideas of the simple one-dimensional mixed-layer models of Kraus and Turner (1967), Niiler (1975), and Niiler and Kraus (1976). The inclusion of inertial accelerations in the momentum balance permits a relaxation, on the scale of the baroclinic Rossby radius of deformation, of the strict Ekman balance between wind stress and Coriolis acceleration in the mixed layer. Earlier models of three-dimensional mixed layers (de Szoeke, 1980) implicitly considered variations on time and space scales so large that the Ekman balance held good and motion in the mixed layer was decoupled from interior motions. The Rossby-radius relaxation scale is well-known in dynamical oceanography: for example, in linear models of coastal upwelling Yoshida (1955) and Allen (1973) used normal-to-shore accelerations to break the Ekman constraint at the coast and determine a scale for the upwelling zone. The Rossby deformation radius $(gh\Delta\rho/\rho)^{1/2}/f$ depends on a mean layer thickness and a density difference, both of which, in a linear adiabatic model, are preset initially and do not vary. The difficulty in a nonlinear model with mixing, entrainment and heating is that these parameters vary with time and in space so that the Rossby deformation radius can itself vary. De Szoeke and Richman (1981), in a unified model of coastal upwelling with a wind-driven, heated, surface mixed layer, sidestepped this difficulty by heuristically assuming a form for the wind-driven offshore transport with an arbitrarily prescribed constant relaxation scale at the coast. In this paper we present a careful formulation of the momentum balance across regions of strong horizontal gradient and derive, for velocity in the direction of the gradient, an equation [(24), Section 2] that permits the relaxation of the

Ekman-transport constraint on a scale that is determined by the instantaneous distribution of density difference and mixed-layer depth. We illustrate these ideas by applying them in a model of coastal upwelling and mixing, thereby remedying a major deficiency of de Szoeke and Richman's (1981) model.

In formulating the model, we suppose that there exists a principal direction in which horizontal gradients lie and that variations perpendicular to this direction are small or negligible. Then we distinguish between a vertically uniform, turbulent, surface layer, in which turbulent transport of momentum and buoyancy is paramount, and an internal quiescent layer with no turbulent fluxes, except possibly in a thin frictional layer on the bottom (Fig. 1). The boundary between the surface and internal layers is not a material surface, for the upper layer is permitted to entrain the lower. This feature is essential because a material surface under the influence of continual divergence would inevitably surface due to upwelling (Hurlburt and Thompson, 1973; Csanady, 1982). But in an entraining layer, in which entrainment is formulated to be inversely proportional to layer depth, this surfacing can never happen. Instead, upwelled interior water, only slightly diluted by mixing with lighter, former surface water, can appear at the surface, marked from the 'true' interior by only the slightest of density differences in the vertical. However, within the surface layer, which is permitted to sustain horizontal density gradients, a strong front can form between the initial light surface water, now pushed aside by the divergent circulation, and the upwelled interior water.

As these density contrasts develop and the mixed-layer depth changes, the dynamical scale on which the circulation adjusts—the Rossby radius of deformation—varies. Where the density difference between layers is moderately large, traditional estimates of O(10 km) for this adjustment scale are obtained. However, in the water upwelled by the divergent circulation, in which vertical density differences may be slight, this scale can be very small, O(100 m), and determines, among other things, the width of the front between the upwelled water and the former surface water.

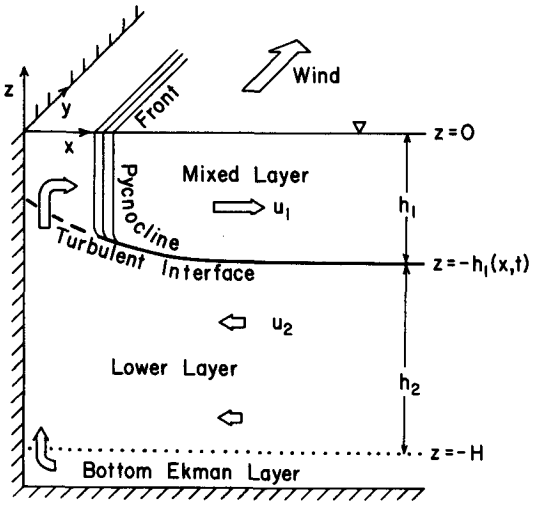

FIG. 1. A sketch of the model geometry, showing some of the principal dynamical features.

The work we describe represents a theoretical advance in that it achieves an analytical formulation in two dimensions of the equations for mixed-layer depth, density, and along-gradient horizontal velocity. Only as the last step must these reduced equations be solved numerically. Foo (1981), on the other hand, produced a two-dimensional model of coastal upwelling that generated a surface front. He did this by numerically integrating the 'primitive' equations of motion formed in terms of isopycnal coordinates. Similarly, Thompson (1978) ran numerical models of coastal upwelling with parameterized mixing processes. The numerical approach has the advantage that it is readily capable of generalization and incorporation of additional effects. It is often said, then, that such models can achieve greater 'realism.' With the analytical approach, by contrast, though it is more difficult and less general, the mathematical structure of the reduced equation set is usually more transparent so that the nature of the solutions can be more easily discerned and described. This often affords deeper physical insight into the more complicated situation occurring in nature, despite the simplifications and limitations of the analytical analogue.

2. Formulating the model

Consider a model of an ocean consisting of two layers, a mixed layer and a lower layer, each homogeneous in the vertical, of constant total depth H. We permit all variables, velocity components, density and pressure, to depend on only one horizontal coordinate, say x. Call the other horizontal coordinate y, and the vertical coordinate z. The equations of motion for the two layers are

$$fv_1 = \rho^{-1}(\overline{p_{1x}}), \tag{1}$$

$$v_{1t} + u_1 v_{1x} + fu_1 = \rho^{-1}\partial\tau_1{}^y/\partial z = (\tau_0{}^y - \tau_e{}^y)/\rho h_1, \tag{2}$$

$$u_{1x} + w_{1z} = 0, \tag{3}$$

$$fv_2 = \rho^{-1}p_{2x}, \tag{4}$$

$$v_{2t} + u_2 v_{2x} + fu_2 = \rho^{-1}\partial\tau_2{}^y/\partial z = 0, \tag{5}$$

$$u_{2x} + w_{2z} = 0. \tag{6}$$

Subscripts 1 and 2 refer to the upper and lower layers, respectively. Horizontal velocity is taken to be vertically uniform within each layer. Flows along isopleths of property distributions are taken to be larger than flows across the isopleths, $v_1 \gg u_1$, $v_2 \gg u_2$, so that the cross-isopleth momentum balance is approximately geo-

strophic. This assumption is called the *semigeostrophic* approximation (Hoskins 1975); a full discussion of it can be found in Pedlosky (1979). It can be valid for time scales as short as $f^{-1}\delta$, where δ is the ratio of cross-isopleth to along-isopleth velocity scales, without upsetting the approximate geostrophic cross-isopleth momentum balance. Its major dynamical effect is the complete filtration of inertio-gravity waves.

Figure 1 illustrates a situation where the orientation of a lateral boundary, a coastline at $x = 0$, prescribes the direction of property distribution gradients. Indeed, it is to this example of coastal circulation that we shall refer the subsequent derivation of the model: henceforth we shall call the cross-isopleth and along-isopleth directions, normal-to-shore and alongshore, respectively. However, nothing in our theoretical development, except a no-normal-flow condition at the coast, is specific to the coastal context, and could apply to any surface-oceanic situation where property distribution isopleths are parallel with small curvature.

Integration of the hydrostatic equation gives, for the pressure field in each layer,

$$p_1 = p_0(x, t) - gz\rho_1(x, t), \quad 0 < -z < h_1, \tag{7}$$

$$p_2 = p_0(x, t) - gh_1(x, t)[\rho_2 - \rho_1(x, t)] - g\rho_2 z, \quad h_1 < -z < H, \tag{8}$$

where $p_0(x, t)$ is the surface pressure (equivalent to a sea surface elevation), $\rho_1(x, t)$ is the variable density of the upper layer, and ρ_2 is the constant lower layer density. Longshore momentum is driven by the turbulent stress divergence, which is assumed to be zero in the lower layer, and $(\tau_0{}^y - \tau_e{}^y)/\rho h_1$ in the upper layer where $\tau_0{}^y$ is the wind stress and $\tau_e{}^y$ the interfacial entrainment stress (about which more later). Notice that (7) is inconsistent with the assumption of vertically uniform flow in the upper layer because $p_{1x} = p_{0x} - gz\rho_{1x}$ contains a z-dependent part. We overcome this by replacing p_{1x} in (1) by its vertical average through the mixed layer

$$(\overline{p_{1x}}) = p_{0x} + \tfrac{1}{2} gh_1\rho_{1x}, \tag{9}$$

while

$$p_{2x} = p_{0x} - g[h_1(\rho_2 - \rho_1)]_x. \tag{10}$$

This procedure can be justified by a cumbersome expansion of upper layer variables in terms of a set of orthogonal vertical basis functions, the first two of which are 1 and $(z + \frac{1}{2}h_1)$. On the assumption that higher-order coefficients in such an expansion are progressively smaller, the lowest order coefficients can be shown to satisfy approximately the equation set (1)–(3), with (9) used on the right side of (1).

Continuity Eqs. (3) and (6) can be integrated down from the surface, where vertical velocity vanishes, and up from the bottom, where vertical velocity is given by Charney's consistency relation

$$w_B = lv_{2x}, \quad l = \left(\frac{A}{2f}\right)^{1/2}, \tag{11}$$

A being a vertical eddy exchange coefficient associated with a thin bottom Ekman layer. This gives for the vertical velocity on either side of the layer interface, $z = -h_1$,

$$(w_1)_i = h_1u_{1x}, \quad (w_2)_i = -h_2u_{2x} + w_B, \tag{12}$$

where $h_1 + h_2 = H$, constant. These vertical velocities are not identical; rather, *normal* velocity at the interface must be continuous,

$$u_1h_{1x} + (w_1)_i = u_2h_{1x} + (w_2)_i, \tag{13}$$

so that

$$(h_1u_1)_x = -(h_2u_2)_x + w_B. \tag{14}$$

The latter may be integrated to give, using $u_1 = u_2 = 0$ at $x = 0$,

$$h_1u_1 + h_2u_2 = \int_0^x w_B dx. \tag{15}$$

The vertical entrainment velocity, w_e, the mean rate at which material is crossing the layer interface, is the difference between the 'apparent motion,' $-Dh_1/Dt$, and particle motion w_i at the interface, and can be written (de Szoeke, 1980)

$$\begin{aligned} w_e = (Dh_1/Dt + w)_i &= h_{1t} + u_1h_{1x} + (w_1)_i \\ &= h_{1t} + u_2h_{1x} + (w_2)_i \\ &= h_{1t} + (u_1h_1)_x. \end{aligned} \tag{16}$$

The third equality, which follows from (13), shows that the kinematic definition of entrainment velocity is well-posed despite discontinuities of velocity at the interface.

The rate of momentum deficit transfer, called the entrainment stress, to the upper mixed layer because of entrainment of lower layer water of differing velocity is (de Szoeke, 1980)

$$\tau_e{}^y = \rho(v_1 - v_2)w_e. \tag{17}$$

Negligible turbulent stress in the lower layer is assumed. The normal-to-shore entrainment stress can be similarly defined, but is held to be negligible in the normal-to-shore momentum balance (1).

The appearance of upper layer density $\rho_1(x, t)$ as a variable, rather than being prescribed as in conventional two-layer models, requires the specification of the heat balance in the upper layer.[1] In terms of density, this can be written

$$\rho_{1t} + u_1\rho_{1x} = [-\alpha Q_0/c - (\rho_1 - \rho_2)w_e]h_1{}^{-1}, \tag{18}$$

where Q_0 is the surface heat transfer from the atmosphere (positive when downward), and α, c are the

[1] With little extra trouble, the dependence of density on the salt balance could also be specified.

thermal expansibility and heat capacity at constant pressure of water. The term $(\rho_1 - \rho_2)w_e$ is the rate of transfer of density deficit from the lower layer to the upper because of entrainment, or entrainment density flux, analogous to the entrainment stress (17).

It remains to specify w_e. In nonentraining two-layer models it is assumed that $w_e \equiv 0$ in (16)–(18). In general, entrainment rate must depend on the rate of turbulent generation by the wind, on upper layer thickness h_1 and the interfacial density jump $(\rho_2 - \rho_1)$, and on interfacial shear $(v_1 - v_2)$. Kraus and Turner (1967) proposed an argument for relating these qualities. The rate of working of turbulent fluctuations of buoyancy and velocity against gravity, given by

$$\int_{-h_1}^{0} g\overline{w'\rho'}dz = \tfrac{1}{2} gh_1[(\rho_2 - \rho_1)w_e + \alpha Q_0/c], \quad (19)$$

serves to increase the potential energy of the mixed layer. This increase must be supplied by the working of the wind upon the water, for which Kraus and Turner (1967) suggested the simple form $m_0\rho u_*^3$, where $u_* = (|\tau_0|/\rho)^{1/2}$ is friction velocity in water, as having the required units, namely, power/area. The constant m_0 has a value ~ 0.5, according to observations of mid-ocean mixed-layer deepening (Davis *et al.*, 1981a,b). Shear at the interface has been neglected, though Niiler (1975) has shown how to include it in the analysis (see also Niiler and Kraus, 1976; de Szoeke and Rhines, 1976; de Szoeke, 1980). Certainly, there are situations in which this neglect cannot be justified (Price *et al.*, 1978), but we shall persist with it for the sake of simplicity. With Kraus and Turner's parameterization, entrainment velocity is given as

$$w_e = \frac{m_0\rho u_*^3 - \frac{1}{2} g\alpha c^{-1} h_1 Q_0}{\frac{1}{2} gh_1(\rho_2 - \rho_1)}. \quad (20)$$

This completes the formal specification of the model equations.

A little manipulation yields some illuminating simplifications. First, subtract (4) from (1), using (9), (10), to obtain the thermal wind balance:

$$\rho f(v_1 - v_2) = g(\rho_2 - \rho_1)h_{1x} - \tfrac{1}{2} gh_1\rho_{1x}. \quad (21)$$

This eliminates the unknown surface pressure $p_0(x, t)$. Next subtract (5) from (2):

$$(\partial_t + u_1\partial_x)(v_1 - v_2) + (f + v_{2x})(u_1 - u_2) = \frac{\tau_0^y - \tau_e^y}{\rho h_1}. \quad (22)$$

Using (15),

$$u_1 - u_2 = [1 + h_1/(H - h_1)]u_1 - (H - h_1)^{-1}\int_0^x w_B dx. \quad (23)$$

Eq. (21) can be substituted into (22) to eliminate $(v_1 - v_2)$. This yields terms involving time derivatives of h_1 and $(\rho_2 - \rho_1)$, which can be eliminated by using (16) and (18). Manipulation and use of (17) and (20) for τ_e^y and w_e leads to a diagnostic equation for u_1, that is, one involving no time derivatives:

$$-f^{-1}(\rho^{-1}gh_1^2(\rho_2 - \rho_1)u_{1x})_x + h_1 P\left[Hu_1 - \int_0^x w_B dx\right] = \tau_0^y/\rho - f^{-1}\partial_x(m_0 u_*^3), \quad (24)$$

where $P = (f + v_{2x})/(H - h_1)$ is the potential vorticity of the lower layer. Note that $w_B = I[P(H - h_1) - f]$.

An equation for P is obtained by differentiating (5) with respect to x, substituting (6) to eliminate u_{2x}, then using $w_{2z} = [(w_2)_i - w_B]/(H - h_1)$, with w_B, $(w_2)_i$ given by (11) and (16). The result is

$$(\partial_t + u_2\partial_x)P = P\frac{w_e - w_B}{H - h_1}. \quad (25)$$

Eqs. (16) and (18) can be rewritten as

$$(\partial_t + u_1\partial_x)[h_1(\rho_2 - \rho_1)] = -u_{1x}h_1(\rho_2 - \rho_1) + \alpha Q_0/c, \quad (26)$$

$$(\partial_t + u_1\partial_x)h_1 = -u_{1x}h_1 + w_e, \quad (27)$$

where w_e is given in terms of h_1 and $(\rho_2 - \rho_1)$ by (20). The boundary conditions on (24) are

$$u_1 = 0 \quad \text{at} \quad x = 0, \quad (28)$$

$$u_1 \text{ is bounded as } x \to \infty. \quad (29)$$

If there were no entrainment or heating, $w_e = Q_0 = 0$, so that $(\rho_2 - \rho_1)$ could be taken to be constant, then (26) and (27) degenerate to the same equation. We might neglect the vortex-stretching effects on the lower layer of entrainment and bottom Ekman layer pumping, i.e., neglect the right side of (25). Further, we might neglect relative vorticity v_{2x} compared to planetary vorticity f, and if variations of h_1 are small replace it by a representative average value $\bar{h}_1$ so that

$$P \approx f/(H - \bar{h}_1). \quad (30)$$

Using this in (24) and replacing h_1 everywhere in that equation by $\bar{h}_1$, we obtain

$$-\lambda^{-2}u_{1xx} + u_1 = (\tau_0^y/\rho f\bar{h}_1)[1 + \bar{h}_1/(H - \bar{h}_1)]^{-1}, \quad (31)$$

where

$$\lambda = [\rho^{-1}g(\rho_2 - \rho_1)(\bar{h}_1^{-1} + (H - \bar{h}_1)^{-1})^{-1}]^{1/2}f^{-1} \quad (32)$$

is the baroclinic Rossby radius of deformation. The solution of (31) satisfying (28), (29) is

$$u_1 = \left(\frac{\tau_0^y}{\rho f\bar{h}_1}\right)[1 + \bar{h}_1/(H - \bar{h}_1)]^{-1}(1 - e^{-\lambda x}) \quad (33)$$

for uniform τ_0^y. For $H = \infty$ this is identical with Yo-

shida's (1955) solution for offshore transport in two-layer coastal upwelling. It is also the form we prescribed in our previous study of the effects of entrainment and mixing on coastal upwelling (de Szoeke and Richman, 1981).

Far from the coast either (31) or (24) exhibits the Ekman transport relation,

$$h_1 u_1 = \frac{\tau^y}{\rho f}, \tag{34}$$

while near the coast the balance of terms in (31) and (24) must adjust to the no-flow boundary condition at the coast on a scale of order λ. This is fairly well known for layered or stratified models (Allen, 1973, Yoshida, 1955). The novelty in the equation set (24)–(27) is that the adjustment scale is not determined by an arbitrary prescription of h_1, $\rho_2 - \rho_1$, but, rather, is determined through these variables by the mixing dynamics inherent in Eqs. (26), (27).

Equations (26), (27) can be solved by the method of characteristics. The characteristics $x_1(t, \xi)$ are given by

$$\frac{dx_1}{dt} = u_1 \quad \text{with} \quad x_1(0, \xi) = \xi. \tag{35}$$

Following the characteristics, (26) and (27) can be written

$$\frac{d}{dt}[h_1(\rho_2 - \rho_1)] = -u_{1x} h_1(\rho_2 - \rho_1) + \frac{\alpha Q_0}{c}, \tag{36}$$

$$\frac{dh_1}{dt} = -u_{1x} h_1 + w_e. \tag{37}$$

Similarly, (25) can be solved by following its characteristics $x_2(t, \xi)$, given by

$$\frac{dx_2}{dt} = u_2 \quad \text{with} \quad x_2(0, \xi) = \xi, \tag{38}$$

where u_2 is determined from u_1 and the other variables by (23). Following these, (25) can be written

$$\frac{dP}{dt} = P\frac{w_e - w_B}{H - h_1}. \tag{39}$$

Equations (35)–(39) can be used to advance the variables h_1, $(\rho_2 - \rho_1)$, P one time step Δt from current values on a grid of points moving according to (35) and (38) and identified by their initial positions $\{\xi_i\}$. Then Eq. (24), since it contains no time derivatives, can be solved in finite-difference form to obtain a new distribution of u_1 from the given h_1, $(\rho_2 - \rho_1)$, P.

3. Scaling

It is instructive to scale the dimensional equations (24)–(27) [or, in characteristic form, (24) and (35)–(39)]. We make the following substitutions.

Driving functions:

$$\tau_0{}^y = \rho u_*^2 \tau', \quad Q_0 = Q_* Q', \tag{40a}$$

Independent variables:

$$x = \lambda_* x', \quad t = t_* t', \tag{40b}$$

Dependent variables:

$$h_1 = h_* h, \quad \rho_2 - \rho_1 = \rho_* \Delta, \tag{40c}$$

$$(u_1, u_2) = V_*(u_1', u_2'), \tag{40d}$$

$$P = P_* P'. \tag{40e}$$

The dimensional scales, indicated by asterisk subscripts, are defined in Table 1; also listed are typical values of the scales for representative settings of the driving forces, wind stress and surface heat flux. The vertical scale is the Monin–Obukhov length h_*. The velocity scale is determined from the balance of Coriolis force with vertical stress divergence. The density scale ρ_* is suggested by comparing horizontal advection of heat with surface heat flux within the surface layer. The choice of time scale renders time-dependent and horizontal-advective effects comparable. The horizontal length scale, if taken to be a Rossby deformation radius based on h_* and ρ_*, is $\lambda_* = (g(\rho_*/\rho_0)h_*)^{1/2}/f$. Substituting for h_* and ρ_* in this definition, we determine that $\lambda_* = 2m_0 u_*/f$ and hence that $\rho_* = 2m_0 \alpha Q_*/cu_*$. Typical values of these scales have been computed and listed in Table 1. The horizontal length scale and density scale are extremely small: 100 m, 3×10^{-4} kg m^{-3}, respectively. These are intrinsic scales. The density scale represents the eventual density differences between layers that can pertain when water upwelling in a narrow layer with depth given by the Monin–Obukhov scale has only a short time to absorb heat through the sea surface before being swept offshore by the Ekman transport. In typical situations in nature, initial density differences of O(1 kg m^{-3}) (corresponding to $\Delta \sim 10^4$) before the onset of upwelling-favorable conditions are normal. This density difference, rather than ρ_*, will initially determine the Rossby deformation scale which sets the width of the upwelling region. Eventually, however, this large initial density difference will be wiped out by the upwelling and will tend to something of order ρ_* at the same time as the upwelling zone shrinks to a width of order λ_*. The questions are still open of how long this process can take, and of the nature of the spatial transition between the nearshore upwelling region and the offshore region. These questions and others are addressed in the numerical solutions obtained and discussed in the next section.

Using the scaling of (40) and Table 1, we can rewrite (24)–(27):

$$-(h^2 \Delta u_{1x})_x + hP\left\{u_1 - E^{1/2}\int_0^x [P(1 - \delta h) - 1]dx'\right\} = \tau - \frac{1}{2}\frac{\partial}{\partial x}\tau^{3/2}, \tag{41}$$

TABLE 1. Dimensional variables and their dimensional scales, with typical values calculated for representative settings of the driving functions.

Variable	Scale; relation to driving scales	Typical value
(A) *Driving functions*		
Wind stress τ_0^y	ρu_*^2	0.1 N m^{-2}
Friction velocity u_*		1 cm s^{-1}
Surface heat flux Q_0	Q_*	75 W m^{-2}
(B) *Independent variables*		
Horizontal distance x	(a) $\lambda_* = (g(\rho_*/\rho)h_*)^{1/2}/f$ $= 2m_0u_*/f$†	100 m
	(b) $\lambda_0 = (g(\Delta_i\rho_*/\rho)h_ih_*)^{1/2}/f$ $= (\Delta_ih_i)^{1/2}\lambda_*$ (Rossby deformation radii)	
Time t	$t_* = h_*(u_*^2/f\lambda_*)^{-1}$ $= h_*(2m_0u_*)^{-1}$	3300 s
(C) *Dependent variables*		
Mixed-layer depth h_1	$h_* = m_0u_*^3/(\frac{1}{2}\alpha gQ_*/c\rho)$‡ (Monin–Obukhov length)	33 m
Density difference $\rho_2 - \rho_1$	$\rho_* = \lambda_*(\alpha Q_*/c)(u_*^2/f)^{-1}$ $= 2m_0\alpha Q_*/cu_*$	3×10^{-4} kg m^{-3}
Horizontal velocities u_1, u_2	$V_* = u_*^2/fh_*$	3 cm s^{-1}
Potential vorticity P	$P_* = f/H$§	3×10^{-7} m^{-1} s^{-1}

† Coriolis parameter $f = 10^{-4}$ s^{-1}, mixing efficiency $m_0 = 0.5$ (Davis *et al.*, 1981a,b).
‡ Thermal expansibility $\alpha = 1.7 \times 10^{-4}$ °C^{-1}, gravity $g = 9.8$ m s^{-2}, specific heat of water at constant pressure $c = 4.1 \times 10^3$ J kg^{-1} °C^{-1}, water density $\rho = 10^3$ kg m^{-3}.
§ Total water depth $H = 330$ m.

$$(h\Delta)_t + (h\Delta u_1)_x = Q, \tag{42}$$

$$h_t + (hu_1)_x = w_e, \tag{43}$$

$$P_t + u_2P_x = P\frac{\delta w_e - E^{1/2}[P(1-\delta h) - 1]}{1 - \delta h}, \tag{44}$$

(having dropped the primes) where $\delta = h_*/H$, and $E = l^2/H^2 = A/2fH^2$ is the bottom Ekman number. Also

$$w_e = \frac{\tau^{3/2} - hQ}{h\Delta}, \tag{45}$$

$$u_2 = -\frac{\delta hu_1}{1-\delta h} + E^{1/2}(1-\delta h)^{-1} \times \int_0^x [P(1-\delta h) - 1]dx'. \tag{46}$$

For a total depth of $H = 330$ m, $\delta = 0.1$; and for a bottom Ekman layer depth of $l = 10$ m, corresponding to $A = 2 \times 10^{-2}$ m^2 s^{-1}, the Ekman number is $E = 9.2 \times 10^{-4}$.

To complete the specification of the problem we require the boundary conditions,

$$u_1 = 0 \quad \text{at} \quad x = 0, \tag{47a}$$

$$u_1 \text{ bounded as } x \to \infty \tag{47b}$$

[similar conditions automatically apply to u_2 through (46)]; and initial conditions

$$h(x, 0) = h_i, \quad \Delta(x, 0) = \Delta_i, \quad P(x, 0) = P_i. \tag{48a,b,c}$$

Although there is no difficulty in letting them be spatially variable, we shall choose h_i, Δ_i, P_i constants. To preclude initial alongshore motion, we set $P_i = 1/(1 - \delta h_i)$.

4. The onset and establishment of upwelling: A case study

In this section we describe the onset of upwelling using the model incorporating consistent momentum

dynamics. We show quantitatively how the pycnocline upwells to the surface and then moves offshore as a front between cold, dense, upwelled water and warm, light, surface water offshore. A surprising result is the narrowness, typically several hundred meters, of the active upwelling zone, whereby we mean the region of actual motion divergence adjacent to shore.

Numerical results. The governing equations (41)–(48) were solved numerically by the method of characteristics outlined above. The solutions were obtained nondimensionally using the scaling of the previous section. Hence, in discussing them we shall state nondimensional values of variables. To facilitate comparison with typical situations in nature, however, we shall also indicate, in brackets, the dimensional values corresponding to the setting of parameters in Table 1. We shall display results for initial nondimensional [dimensional] values for mixed-layer depth, density difference, and lower-layer potential vorticity of

$$h_i = 0.5\ [16.5\ \text{m}], \quad \Delta_i = 10^4\ [3\ \text{kg m}^{-3}],$$

$$P_i = 1.05\ [3.0 \times 10^{-7}\ \text{m}^{-1}\ \text{s}^{-1}].$$

These values determine the initial Rossby radius of deformation,

$$\lambda_0 = (gh_ih_*\Delta_i\rho_*/\rho)^{1/2}f^{-1} = (h_i\Delta_i)^{1/2}\lambda_*,$$

which is $71\lambda_*$, or 7.1 km, dimensionally. This scale determines the initial e-folding distance for offshore velocity u_1. In Fig. 2 we show a sequence of normal-to-shore profiles of the dependent variables u_1, h, Δ, P. Dimensional scales for each variable are shown. The times after initiation of the sequence are: (a) 3.5 [3.2 h], (b) 10.6 [9.7 h], (c) 17.7 [16.2 h], (d) 24.7 [22.4 h]. In this sequence the initial values of Δ and P are scarcely altered. In the first member of the sequence, h is scarcely different from a uniform value of 0.5 [17 m]. The scale over which the wind-driven offshore Ekman transport adjusts to zero at the coast is λ_0. As we run through the sequence from (a) to (d) h gradually shoals due to upwelling. Because of the immense value of Δ, entrainment w_e [Eq. (45)] is negligible throughout this period until panel (d) when the surface density is slightly diluted at the shore, so that Δ is decreased. As h shoals the effective Rossby radius is reduced, as can be seen by the tightening of the scale on which u_1 adjusts. In the last member of the sequence (d), h is nearly, though not quite, zero and u_1 changes very abruptly at the shore. The tick marks along the bottom of this and subsequent figures indicate the instantaneous locations of the moving grid points. The abrupt features in the solutions are always adequately resolved.

We can readily calculate a scale for the time taken for this "surfacing" of the layer interface. Vertical velocity at the coast is scaled by an aspect ratio times the horizontal velocity scale u_*^2/fh_*, namely

$$W = \frac{u_*^2}{f\lambda_0} = (h_i\Delta_i)^{-1/2}\frac{u_*^2}{f\lambda_*}.$$

The dimensional time taken to traverse the mixed layer vertically is

$$\frac{h_ih_*}{W} = h_i^{3/2}\Delta_i^{1/2}t_*,$$

which calculation shows it to be 33 h. Though this is substantially larger than the 23 h that the computed solutions indicate, probably because W is an underestimate of the vertical velocity during the later stages when the layer depth is small and the effective Rossby radius is smaller than estimated here, this scaling argument serves to emphasize that the rapid shoaling phase of the inshore mixed layer is unaffected by entrainment and depends only on the initial values, Δ_i and h_i.

The next sequence of profiles, Fig. 3a–h, shows, on greatly expanded horizontal scale and very densely spaced in time, the development of the situation as h approaches zero inshore. We see from the mixed-layer deepening Eq. (45) that, for some sufficiently small value of h, entrainment w_e becomes important despite the initial immensity of Δ, and from (43), (42) that this subsequently must tend to increase h and decrease Δ as entrained dense water quickly dilutes the surface water and increases its density almost to that of the lower layer. It is at this time and in this place that the density and horizontal length scales in Table 1 become relevant. We see this process in the rapid sequence of Fig. 3; all seven panels cover a time change of only 0.24 [0.22 h]. Though the increase of h at the shore is not apparent until panel (d), we see plainly the sudden precipitous decrease of Δ from $\sim 10^4$ [3 kg m^{-3}] to ~ 1 [3×10^{-4} kg m^{-3}] on a length scale of λ_* [=100 m]. From panel (e), t = 24.75 [22.69 h], to panel (h), t = 24.85 [22.78 h], h increases to 0.5 [17 m] at shore, and thereafter remains steady. The adjustment region for u_1 at the coast (initially λ_0 [=7 km] in Fig. 2a shrinks to λ_* by the time of panel (b). On Fig. 2d, or even Fig. 4b, the u_1-profile appears discontinuous; but Fig. 3 shows that it is indeed smooth if the λ_*-scale is resolved. Virtually all of the upwelling now takes place in this narrow zone at the shore. The later panels of Fig. 3 show that the upwelled water begins to form a widening and deepening pool in the surface layer, marked at its outer boundary by the contrast in Δ between dense, cool, upwelled water (~ 1 [3×10^{-4} kg m^{-3}]) and light, warm, offshore water ($\sim 10^4$ [3 kg m^{-3}]). This density contrast, or front, is in fact the pycnocline, formerly synonymous with the turbulent interface between the layers, now upwelled to the surface and being advected offshore. Inshore of the front the turbulent interface is still marked by h, though the water is virtually homogeneous; the small density variations predicted would be nearly immeasurable in nature.

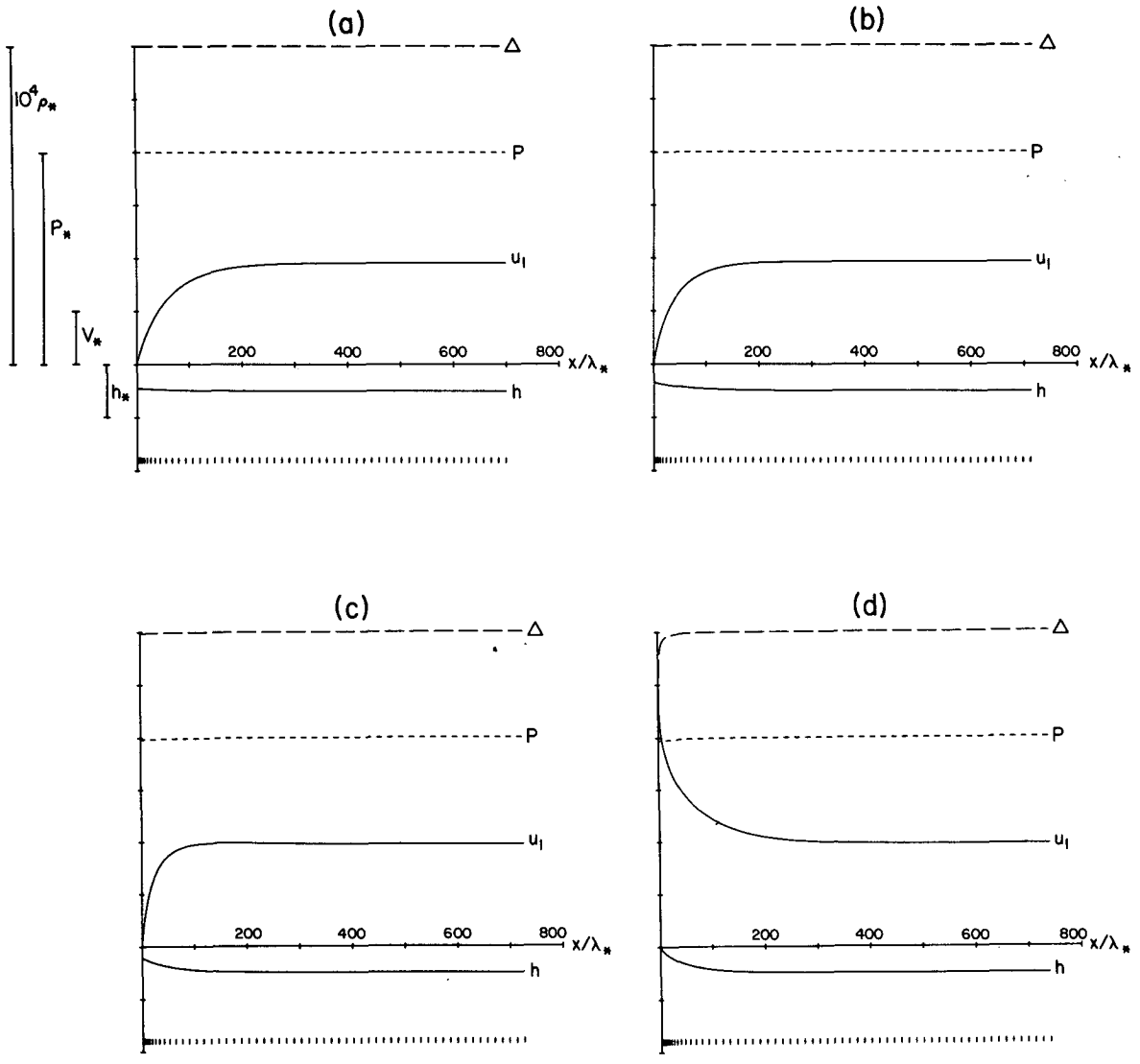

FIG. 2. The pre-upwelling phase. Normal-to-shore profiles of the numerical solutions for mixed layer depth h, density difference Δ, offshore velocity u_1, and lower layer potential vorticity P at the nondimensional [dimensional] times (a) 3.5 [3.2 h], (b) 10.6 [9.7 h], (c) 17.7 [16.2 h], and (d) 24.7 [22.7 h]. The dimensional scales marked on the left of panel (a) are defined in Table 1, where typical values are also given.

Hence, we can distinguish four zones: (i) an Upwelling Zone, (ii) an Upwelled Region, (iii) an Upwelled Front, and (iv) a Warm Offshore Region.

Figure 4a–h shows the further development of these zones on medium time and space scales; note the increase of time step after panel (e). After the time of panel (c) 25.1 [23.0 h], h increases in a short distance from 0.5 [17 m] at the shore to a maximum value offshore. This value approaches the Monin–Obukhov depth 1 [33 m] soon after panel (g), $t = 31.8$ [29.2 h], within a distance of ~ 7 [0.7 km] from shore. We take this maximum depth to define the outer edge of the Upwelling Zone. Within the Zone, divergence is large and positive, as its name suggests, and conditions are steady in time after 31.8 [29.2 h], with entrainment just balancing the divergence. Potential vorticity of the lower layer is increased in the Upwelling Zone by the intense vortex stretching associated with the entrainment.

Farther out, we see the Upwelled Region continually widening. Its thickness declines with distance offshore to join rather abruptly onto the offshore mixed layer depth at the Upwelled Front. The variation of offshore velocity u_1 through the Upwelled Region and the Front into the Offshore Region is roughly inverse to the variation of h, so that transport hu_1 is approximately 1 [1 $m^2\ s^{-1}$]—the Ekman balance. More precisely, there is weak convergence of transport, $(hu_1)_x < 0$, or downwelling, on the cold inshore edge of the Upwelled Front, and weak divergence, $(hu_1)_x > 0$, or upwelling, on the

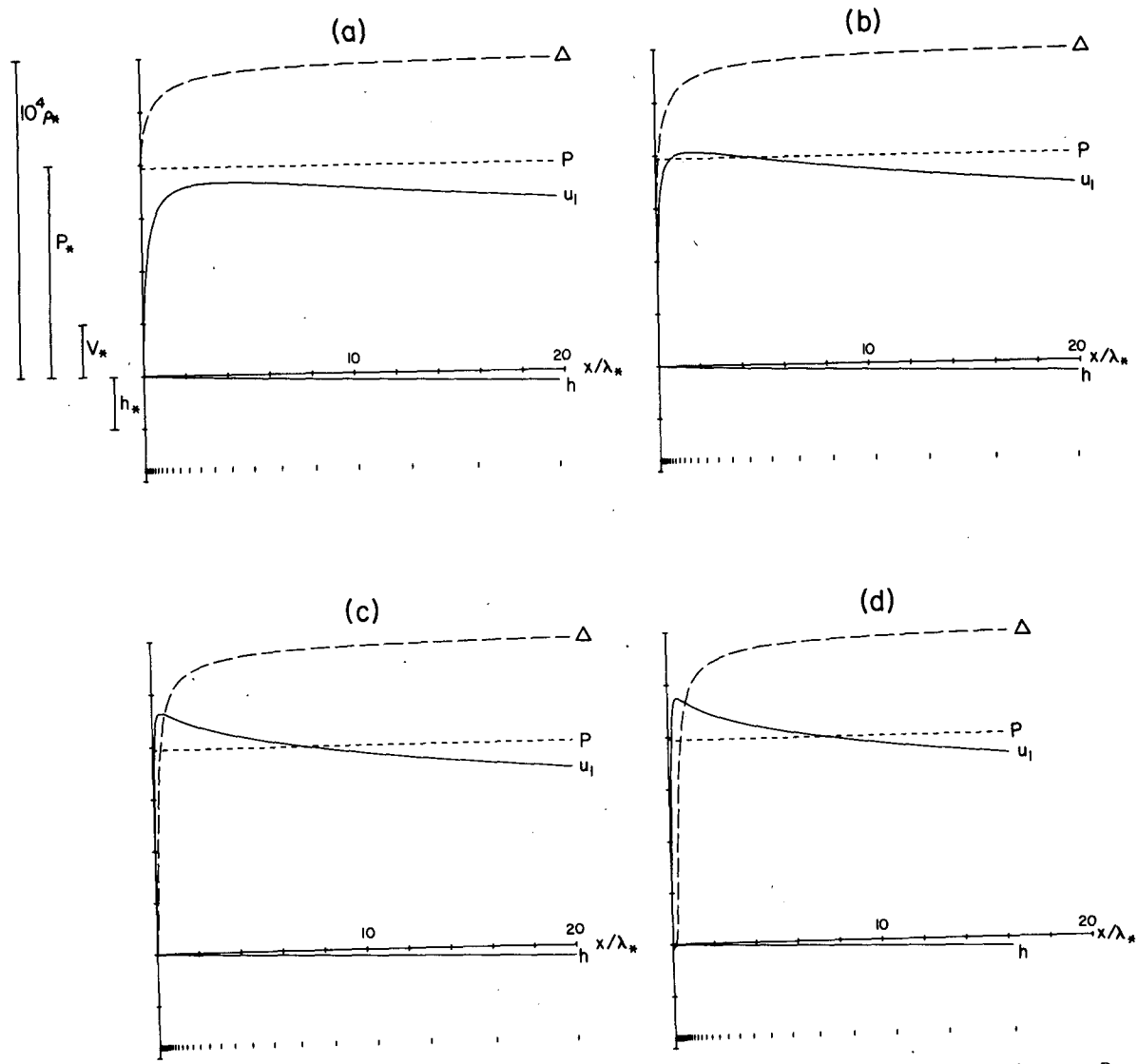

FIG. 3. The eruption of the pycnocline at the shore. Normal-to-shore profiles of the numerical solutions for h, Δ, u_1, P at the times (a) 24.61 [22.56 h], (b) 24.64 [22.59 h], (c) 22.68 [22.62 h], (d) 24.71 [22.65 h], (e) 24.75 [22.69 h], (f) 24.78 [22.72 h], (g) 24.82 [22.75 h] and (h) 24.85 [22.78 h]. Note the expanded horizontal scale. Scales are defined in Table 1.

warm seaward edge of the Front. This feature rather resembles the double-gyre cell that Mooers, *et al.* (1976) discerned in the Upwelled Front on the Oregon shelf.

The Upwelled Front moves offshore with the mixed layer velocity u_1 associated with the minimum layer thickness at the Front. Fig. 5 shows the offshore motion of the Front for two different initial stratifications, $\Delta_i = 10^4$ [3 kg m^{-3}] and $\Delta_i = 10^3$ [0.3 kg m^{-3}]. For both cases, initial mixed layer depth h_i was 0.5 [17 m]. This figure illustrates the fact noted earlier that the time of surfacing of the front is $h_i^{3/2}\Delta_i^{1/2}t_*$. The surfacing time of the weaker stratification is earlier than that of the stronger by a factor of $10^{-1/2}$. Entrainment commences when the mixed layer is deeper for the weaker initial density jump because less potential energy is required to entrain lower layer fluid into the mixed layer. Because the mixed layer depth at the Front is thicker, the weaker Front moves offshore proportionately more slowly. For both cases, the speed of propagation of the Front decreases with time as entrainment slowly deepens the mixed layer in the Front. The frontal speed is asymptotic to V_* (Table 1), which corresponds to a slope of unity in Fig. 5.

The offshore march of the Upwelled Front will proceed until interrupted by the cessation of the wind. The Upwelled Region is nearly homogeneous in the vertical and linearly stratified in the horizontal, though this horizontal gradient is scarcely perceptible in Figs. 2–4. The solution in this region approaches the steady state solution obtained by de Szoeke and Richman

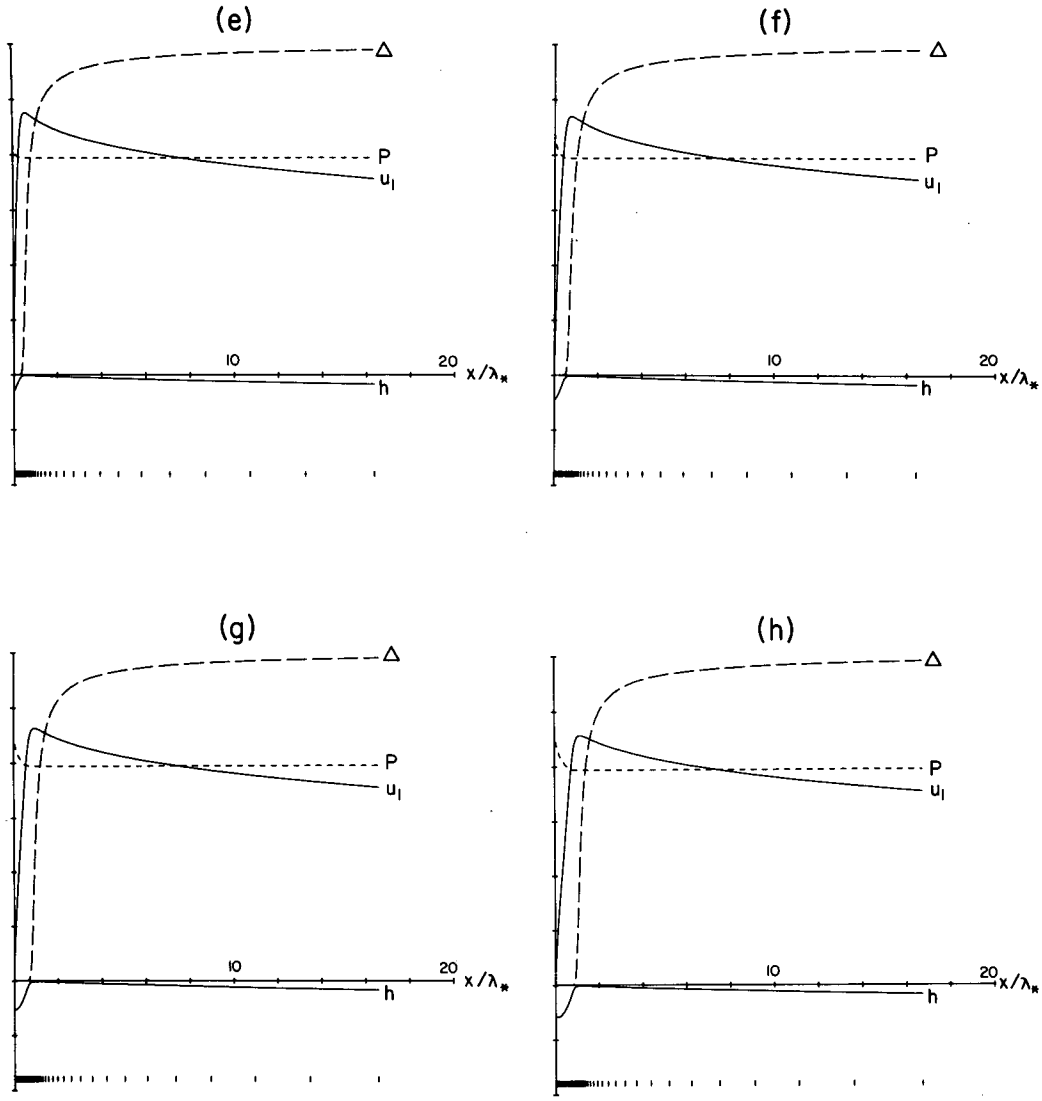

FIG. 3. (*Continued*)

(1981) except that the density and horizontal length scales are the intrinsic scales, ρ_* and λ_*, rather than the initial Rossby deformation radius and corresponding advective density scale. Despite this, the horizontal density gradient scale ρ_*/λ_* is the same as in the previous paper. As the Front progresses offshore the density jump across it diminishes, though, again, this is imperceptible in Fig. 2–4.

Bottom friction. Though it has been incorporated into the formulation of the model, bottom friction has negligible effect on the short-time solutions presented in Figs. 2–5. The effects of bottom friction are felt on much longer times, $O(E^{-1/2})$ pendulum days (Allen, 1973). For an Ekman number of $E = 9.2 \times 10^{-4}$ such as we have been using, this is about 33 pendulum days, compared to about 30 h, the longest time reached on Fig. 4.

The evolutionary role of the bottom Ekman layer can be understood qualitatively as follows. The major effects of bottom friction are twofold: the bottom Ekman layer can balance part (or all) of the offshore transport in the mixed layer (Eq. (15)); and the divergence of this bottom Ekman transport, or 'Ekman pumping', can stretch or squash vortices in the interior lower layer (Eq. (25)), especially near the shore. Moreover, offshore bottom transport implies a longshore bottom stress. In the early-time solutions of Figs. 2–4 these effects are entirely negligible: there is virtually no bottom transport or bottom stress, nor any vortex squashing by bottom Ekman pumping. Because of this, the surface wind stress, not balanced by any bottom stress, must drive a steadily accelerating alongshore barotropic current, and potential vorticity where stretched by entrainment, must steadily increase. The

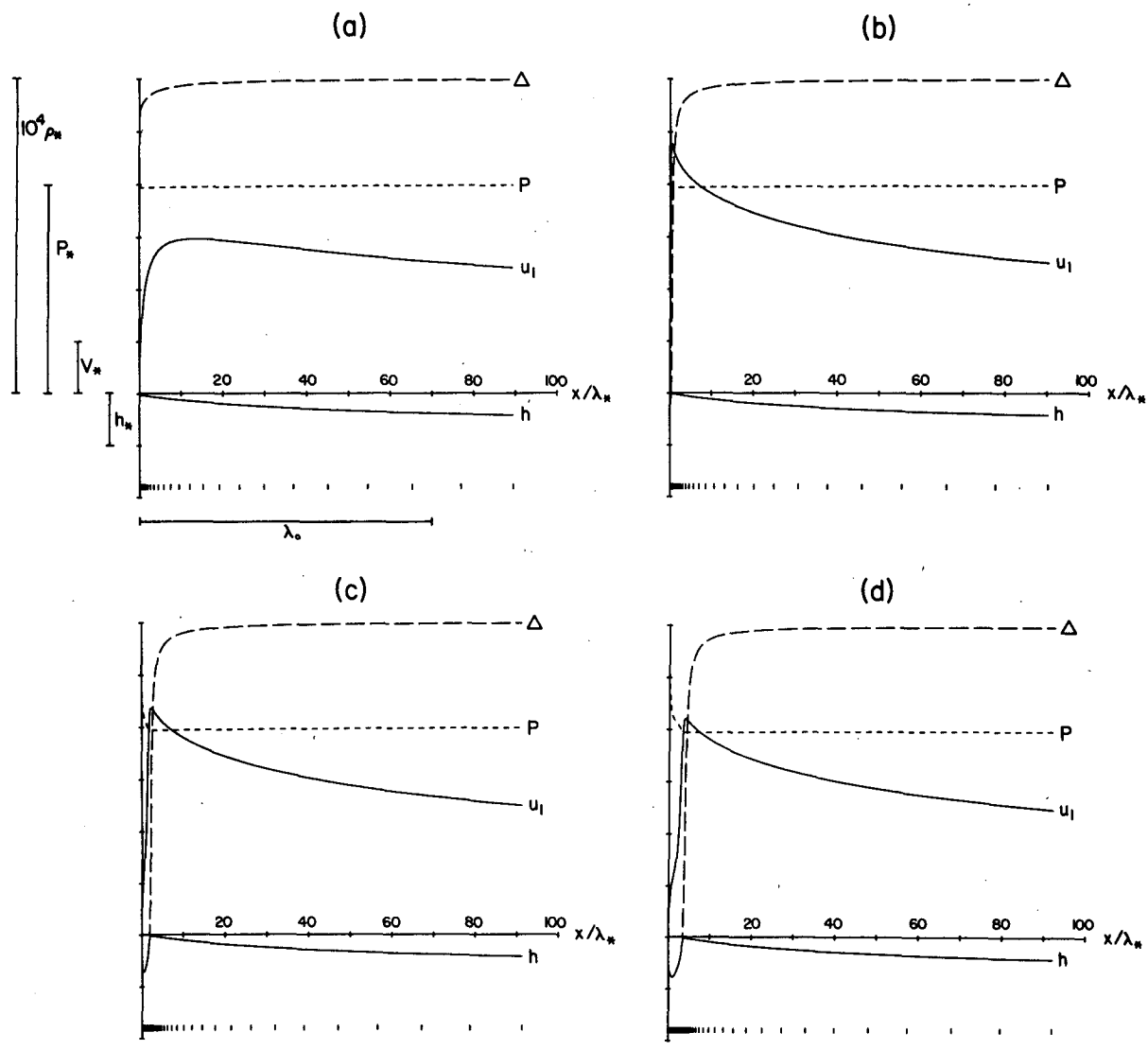

FIG. 4. Mature upwelling; the Front is advected offshore. Normal-to-shore profiles of the numerical solution for h, Δ, u_1, P at the times (a) 24.4 [22.3 h], (b) 24.7 [22.7 h], (c) 25.1 [23.0 h], (d) 25.4 [23.3 h], (e) 25.8 [23.6 h], (f) 28.3 [25.9 h] (g) 31.8 [29.2 h], and (h) 35.4 [32.4 h]. The horizontal scale is intermediate between Figs. 2 and 3. Scales are defined in Table 1.

two effects are related, of course. The increase of potential vorticity in the Upwelling Zone is clearly seen in Figs. 3 and 4. This acceleration and potential vorticity increase ought not to continue forever. In fact, as bottom friction becomes important, the bottom Ekman layer's share of transport, and hence also the longshore bottom stress, increases, thereby reducing the barotropic current acceleration as surface wind stress is transmitted to the bottom. Linked to this is an increasing upward bottom Ekman pumping which counteracts the stretching of lower layer vortices by entrainment and reduces the increase of potential vorticity. Eventually, after $O(E^{-1/2})$ pendulum days, *all* of the mixed-layer transport is balanced by onshore bottom Ekman layer transport, so that surface wind stress is balanced by bottom stress, and longshore acceleration vanishes. Concomitantly, bottom Ekman pumping balances entrainment velocity, vortex squashing and stretching balance, and potential vorticity increase ceases.

This will be the final lower-layer steady state. Whether it is ever achieved in nature is problematic, since it is unlikely that wind stress will hold steady for as long as required. It is different from the steady state that was discussed above for upper-layer depth h, density Δ, and offshore velocity u_1 in the Upwelling Zone and part of the Upwelled Region. This quasi-steady state is reached quite rapidly, as we saw.

The frictional adjustment to the full steady state is fairly well appreciated (Allen, 1973; Pedlosky, 1974).

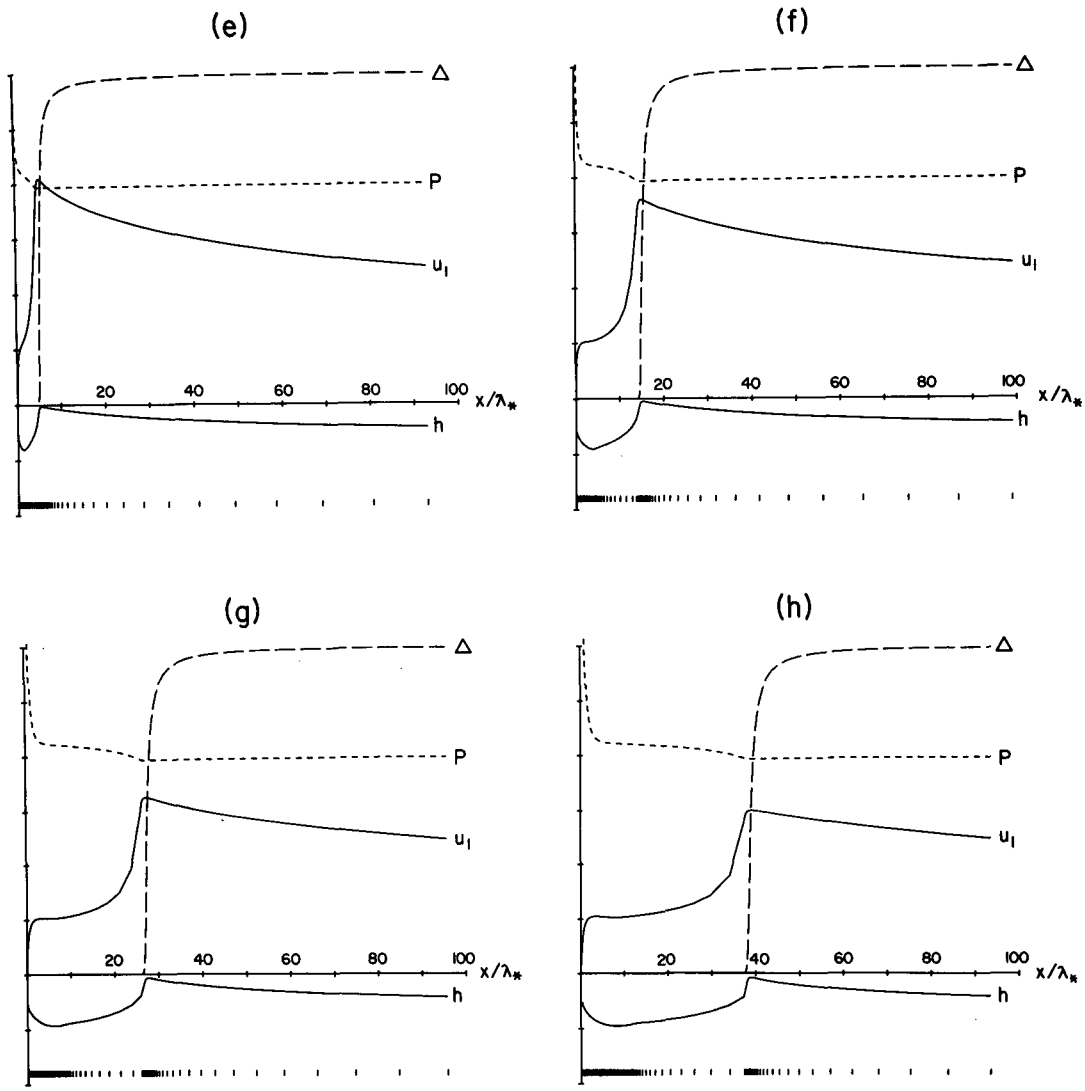

FIG. 4. (*Continued*)

For this reason, the expense and trouble of pushing the numerical solutions of Figs. 2–5 out to the frictional adjustment time scale has not seemed justified.

5. Discussion

We have formed a two-dimensional theory (i.e., one continuous horizontal dimension, layers in the vertical) of wind-driven, diabatic mixing in the surface layer of the ocean in the presence of strong horizontal gradients. Indeed, models based on the theory can spontaneously generate the strong gradients because of its nonlinear character. The analytical development leads to a key equation [(24), Section 2], derived from a careful consideration of momentum balance across the direction of maximum gradient, that permits relaxation of the Ekman balance of Coriolis force against wind stress on short space scales. The proper formulation of this is a prime achievement of the paper. This equation, along with heat balance and entrainment equations for the mixed layer (de Szoeke, 1980), constitutes a reduced set of analytical equations for across-gradient velocity and mixed-layer density and depth, which must be solved numerically.

The theory was applied to a model of alongshore-uniform coastal circulation which was able to mimic features of the onset of wind-driven upwelling quite well. It was able to represent consistently and quantitatively how the pycnocline initially at the layer interface was brought to the surface adjacent to the coast and then advected offshore as an Upwelled Front. Behind the Front was left an extremely narrow Upwelling Zone, several hundred meters wide next to the shore, in which nearly all the actual motion divergence occurred, and between this Zone and the Front, an Upwelled Region, filled with cold dense water brought

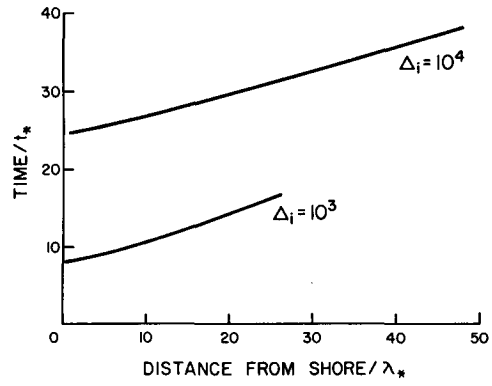

FIG. 5. Location in time of the Upwelled Front for two choices of initial stratification $\Delta_i = 10^4$ [3 kg m^{-3}] and $\Delta_i = 10^3$ [0.3 kg m^{-3}]. For both cases the initial mixed layer depth was $h_i = 0.5$ [17 m]. Scales are defined in Table 1.

up in the Upwelling Zone. The Upwelled Front was not the place where fluid was primarily upwelling. Rather it was a remnant of the onset of upwelling, subsequently advected offshore. In the Upwelling Zone and Upwelled Region a steady state was reached similar to that found by de Szoeke and Richman (1981).

The short time scales of response were also noteworthy: some 20 h for the pycnocline to surface and form the Front, another 10 h for it to move about 5 km offshore. This was for a wind stress of 0.1 N m^{-2}, and a pycnocline of 3 kg m^{-3} at 17 m depth initially.

a. Horizontal scales

The eventual narrowness of the Upwelling Zone was very surprising. At first sight, the extreme narrowness of the 'natural' horizontal scale $\lambda_* = O(u_*/f)$ and the smallness of the associated density scale ρ_* seem troubling. The scaling of Section 3 and the solutions of Section 4 show that the width of the active Upwelling Zone tends to assume this size. In nature, however, coastlines are rarely as smooth as the ideal represented in our theoretical model! Headlands, bays, shoals and canyons projecting several times $\lambda_* \sim 100$ m richly embellish the straightest coastline. The situation is rather similar to boundary-layer turbulence where wall projections larger than the width $O(\nu/u_*)$ of the viscous sublayer (where ν is kinematic viscosity) disrupt its formation. This requires the abandonment altogether of the idea of a viscous sublayer and a theoretical reformulation in terms of a notion of 'hydrodynamic roughness' (Monin and Yaglom, 1971). Clearly, an analogous strategy is called for in the coastal situation, though precisely what form the notion of 'coastal roughness' should take is unclear. One approach we do not favor is the adoption of large lateral eddy viscosities to set a suitably large scale for the motion divergence and the width of the Upwelling Zone: this seems merely to beg the crucial question of the nature of horizontal turbulent transfer processes.

Hence we prefer to offer as it is, though with apologies, our model with an $O(\lambda_*)$-width Upwelling Zone. It serves to show how horizontal scales of variation in upwelling can be controlled by vertical turbulent-transfer processes when vertical density contrasts become small. We note that the dynamics of the processes beyond the Upwelling Zone are pretty independent of it after the formation of the Front and its advection offshore.

The width of the Upwelled Front itself has also been shown to scale as λ_*. This is quite a satisfying result: sharp frontal features are commonly seen in nature in the coastal zones (Mooers *et al.*, 1976). Absent from the theory, however, is any process of frontolysis. Such sharp frontal features should be prone to dynamical instabilities that distort them sinuously in the longshore direction and lead eventually to their diffusion and breakdown. Consideration of such three-dimensional effects is beyond the scope of this paper. Foo (1981) devised a numerical isopycnal-coordinate model of coastal upwelling that produced fronts. His fronts are much less sharp—several kilometers or more wide judging from his published solutions—than ours, indeed his circulation patterns look much smoother than ours, possibly because of large horizontal eddy coefficients.

b. Cross-shelf inertial accelerations

To allay concerns about neglect of inertial accelerations $u_t + uu_x$ in the assumed cross-shelf geostrophic balance (see Eq. (1)) on which this model depends, we computed these terms *ex post facto* from the obtained solutions. Though the neglected terms are largest near the front where gradients are strongest, we found that they never anywhere exceeded 10^{-3} times the retained geostrophic acceleration fv. This shows that the assumed semigeostrophic approximation is consistent with the solution obtained.

c. Neglect of inertial motions

Another effect of neglecting cross-shelf accelerations—one that cannot be checked consistently from the obtained solution—is the complete filtration of inertial oscillations, indeed of the entire internal inertio-gravity wave band. Inertial motions can produce large shears at the mixed-layer base which would enhance mixing (Niiler, 1975). Millot and Crépon (1981) have studied the generation of inertial oscillations on a continental shelf adjacent to a coastline. They found that, at a given distance from the coast, inertial motions are generated by the impulsive onset of wind and last until a Poincaré wave front, issuing from the coast and travelling with internal gravity-wave speed $(gh\Delta\rho/\rho)^{1/2}$, arrives. Thereafter, the inertial motions are nearly precisely cancelled by the near-inertial Poincaré-wave motions. Using $h = 17$ m and $\Delta\rho/\rho = 3 \times 10^{-3}$, the speed of this Poincaré-wave front is 0.7 m s^{-1}, much

faster than the 3 cm s^{-1} or so at which the Upwelled Front advances. Hence after an initial transient, no inertial motions are expected in the vicinity of the coast where the Upwelled Front forms. This seems reasonable for moderately straight coastlines. For more convoluted coastlines and bottom topographies, focussing of inertial waves may occur and result in their persistence nearshore, but this is well beyond the scope of the present paper.

d. Neglect of shear mixing

Niiler (1975) proposed a formulation of one-dimensional mixed-layer dynamics that explicitly incorporated shear production of turbulent kinetic energy into the Kraus and Turner (1967) model. We have not included this effect in our formulation. However, we have checked the size of the bulk Richardson number

$$\mathrm{Ri} = \frac{g\Delta\rho h}{\rho(\Delta u^2 + \Delta v^2)}$$

after the fact from our computed solutions. The smallest Richardson numbers, of order 0.1, occur in the Upwelled Front where $\Delta\rho$ is small, shears are large, and especially, h is small. Were a shear production mechanism to be included in our model, this would lead to enhanced mixing, and hence a deeper minimum mixed layer where the cold upwelled water abuts the warm offshore water. In both the Upwelled Zone and the Warm Offshore Region, Richardson numbers are larger, usually much larger than 1.0, and no stunning qualitative effects ought to be expected from inclusion of a shear production mechanism.

e. Other limitations

Numerous limitations of the theory could be cited. The assumed two-dimensionality is quite fundamental: without it the semigeostrophic approximation could not be made. However, a theory could probably be developed to handle weak alongshore variations. On the other hand, the use of two-layer stratification is not fundamental. Generalization of the analytical theory to several layers is fairly straightforward and amenable to numerical implementation. The effects of normal-to-shore bottom topography could quite readily be included.

Acknowledgments. This research was sponsored by the National Science Foundation under Grant OCE-8117694 and by the Office of Naval Research under Contract N000174-79-C-0004, Project NR 083-102. Eric Beals assisted with the computations. We are grateful to John Allen for useful discussions.

REFERENCES

Allen, J. S., 1973: Upwelling and coastal jets in a continuously stratified ocean. *J. Phys. Oceanogr.*, **3**, 245–257.

Csanady, G. T., 1982: On the structure of transient upwelling events. *J. Phys. Oceanogr.*, **12**, 84–96.

Davis, R. E., R. de Szoeke, D. Halpern and P. Niiler, 1981a: Variability in the upper ocean during MILE. Part I: The heat and momentum balances. *Deep-Sea Res.*, **28**, 1427–1451.

——, ——, and P. P. Niiler, 1981b: Variability in the upper ocean during MILE. Part II: Modeling the mixed layer response. *Deep-Sea Res.*, **28**, 1453–1475.

de Szoeke, R. A., 1980: On the effects of horizontal variability of wind stress on the dynamics of the ocean mixed layer. *J. Phys. Oceanogr.*, **10**, 1439–1454.

——, and P. B. Rhines, 1976: Asymptotic regimes in mixed-layer deepening. *J. Mar. Res.*, **34**, 111–116.

——, and J. G. Richman, 1981: The role of wind-generated mixing in coastal upwelling. *J. Phys. Oceanogr.*, **11**, 1534–1547.

Foo, E., 1981: A two-dimensional diabatic isopycnal model—Simulating the coastal upwelling front. *J. Phys. Oceanogr.*, **11**, 604–626.

Hoskins, B. J., 1975: The geostrophic momentum approximation and the semi-geostrophic approximation. *J. Atmos. Sci.*, **32**, 233–242.

——, and F. P. Bretherton, 1972: Atmospheric frontogenesis models: mathematical formulation and solution. *J. Atmos. Sci.*, **29**, 11–37.

Hurlburt, H. E., and J. D. Thompson, 1973: Coastal upwelling on a β-plane. *J. Phys. Oceanogr.*, **3**, 16–32.

Kraus, E. B., and J. S. Turner, 1967: A one-dimensional model of the seasonal thermocline: II. The general theory and its consequences. *Tellus*, **19**, 98–106.

Millot, C., and M. Crépon, 1981: Inertial oscillations on the continental shelf of the Gulf of Lions—Observations and Theory. *J. Phys. Oceanogr.*, **11**, 639–657.

Monin, A. S., and A. M. Yaglom, 1971: *Statistical Fluid Mechanics*, Vol. 1. Eng. Translation, J. L. Lumley, Ed., M.I.T. Press, 769 pp.

Mooers, C. N. K., C. A. Collins and R. L. Smith, 1976: The dynamic structure of the Frontal zone in the coastal upwelling region off Oregon. *J. Phys. Oceanogr.*, **6**, 3–21.

Niiler, P. P., 1975: Deepening of the wind-mixed layer. *J. Mar. Res.*, **33**, 405–422.

——, and E. B. Kraus, 1976: One-dimensional models of the upper ocean. *Modelling and Prediction of the Upper Layers of the Ocean.* E. B. Kraus, Ed., Pergamon Press, 153–172.

Pedlosky, J., 1974: Longshore currents, upwelling and bottom topography. *J. Phys. Oceanogr.*, **4**, 214–226.

——, 1978: A nonlinear model of the onset of upwelling. *J. Phys. Oceanogr.*, **8**, 178–187.

——, 1979: *Geophysical Fluid Dynamics.* Springer-Verlag, 624 pp.

Price, J. F., C. N. K. Mooers and J. C. Van Leer, 1978: Observation and simulation of storm-induced mixed-layer deepening. *J. Phys. Oceanogr.*, **8**, 582–599.

Thompson, J. D., 1978: Role of mixing in dynamics of upwelling systems. *Upwelling Ecosystems*, R. Boje and M. Tomezak, Eds., Springer-Verlag, 203–222.

Yoshida, K., 1955: Coastal upwelling off the California coast. *Rec. Oceanographic Works Japan*, **2**, 8–20.